JAAS

PAPER

View Article Online
View Journal | View Issue

Cite this: J. Anal. At. Spectrom., 2015, 30, 2412

Particle size-related elemental fractionation in laser ablation in liquid inductively coupled plasma mass spectrometry

Ryo Machida, Takashi Nakazawa, Yuka Sakuraba, Masahide Fujiwara and Naoki Furuta*

Particles sampled by means of laser ablation in liquid (LAL) can be analyzed by inductively coupled plasma mass spectrometry (ICPMS) after acid digestion or slurry nebulization. The LAL sampling process is simple, and a standard solution can be used for calibration. In this study, we investigated elemental fractionation during LAL by using a standard glass reference material, NIST 610. NIST 610 was placed in an open-top chamber, and ultrapure water was added until the surface of the glass was 3 mm below the water surface. LAL sampling was carried out in line-scanning mode. The LAL-sampled particles were divided into two size classes by filtration through a polycarbonate filter: particles larger than 0.4 μm were collected on the filter, and particles smaller than 0.4 μm passed into the filtrate. Both sizes of particles were digested with acid and analyzed by ICPMS. Volatile elements were enriched in the smaller particles and depleted in the larger particles. That is, elemental fractionation related to the size of the ablated particles was observed during the LAL-sampling process. When the LAL-sampled particles were introduced into the ICP, the large particles did not decompose completely. Volatile elements in the larger particles were vaporized more easily than calcium. Therefore, positive elemental fractionation was observed when the LAL-sampled particles were analyzed by slurry nebulization ICPMS. Comparison between slurry nebulization and acid digestion revealed that particle size-related elemental fractionation in the ICP was larger than that observed during LAL sampling.

Received 21st August 2015
Accepted 9th October 2015

DOI: 10.1039/c5ja00349k

www.rsc.org/jaas

1. Introduction

Laser ablation inductively coupled plasma mass spectrometry (LA-ICPMS) is a technique for direct analysis of solid samples without the need for sample preparation procedures; ablated particles are generated by the interaction between laser light and the sample surface. LA-ICPMS has been used for various purposes, such as isotope-ratio analysis in the field of earth science and qualitative analysis of biological tissues and other materials.[1–4] Various quantitative strategies that use LA-ICPMS have been investigated, such as a correction method involving the use of a relative sensitivity factor and a standard addition method.[5–8] However, LA-ICPMS suffers from elemental fractionation, whereby elements in a sample are enriched or depleted during the LA process and in the ICPMS, depending on the properties of the elements. However, the problem of elemental fractionation has not yet been solved. During the laser ablation process, elemental fractionation depends on the laser type, operating conditions, and aspect ratio (depth/diameter) of a crater. Larger elemental fractionation occurs when aspect ratios of the crater increase.[9] On the other hand in the ICP, elemental fractionation occurs when particles larger than a critical size are introduced into the ICP. For example, one hundred fifty nanometers (150 nm) is a critical size for silicates.[10] Shorter laser-pulse durations (*e.g.*, on the order of femtoseconds) and the use of ultraviolet radiation (193 nm) have been investigated for the smaller heat effective zone and the generation of smaller particles.[11–14]

Laser ablation in liquid (LAL) was first reported as a technique for the generation of nanomaterials in 2003, and ablation mechanisms have been widely studied.[15–17] In this technique, the sample surface is irradiated by a laser beam through a liquid medium. Interest in LAL has been increasing recently owing to its versatility. For instance, LAL has been used for surface-enhanced Raman scattering labeling, production of nanomaterial coatings, photonic materials, and catalysis.[18–21] LAL-sampled particles can be analyzed by ICPMS. Although quantitative analysis by means of slurry nebulization and isotope-ratio analysis has been reported,[22,23] quantification of volatile elements such as As has not been reported. The contributions of particle size-related elemental fractionation during LA and in the ICP have not been clarified. Although slurry nebulization is useful for quantitative analysis,[24–26] the analysis is carried out on the assumption that the particles decompose completely in the

Faculty of Science and Engineering, Department of Applied Chemistry, Chuo University, 1-13-27 Kasuga, Bunkyo-ku, Tokyo 112-8551, Japan. E-mail: nfuruta@chem.chuo-u.ac.jp; Fax: +81-3-3817-1906; Tel: +81-3-3817-1906

ICP. However, large particles do not in fact decompose completely, and the extent of vaporization and atomization of the elements in the particles depends on the elemental properties.[27,28] If these effects could be elucidated, ICPMS analysis with LAL sampling could be an effective tool for the determination of trace elements in hard-to-digest materials, such as glass and fine ceramics.

In this study, elemental fractionation during LAL sampling was investigated separately from elemental fractionation in the ICP. Particle size-related elemental fractionation during LAL sampling was evaluated by comparison between LAL-sampled particles larger than 0.4 μm and those smaller than 0.4 μm, and elemental fractionation in the ICP was evaluated by comparison between the results obtained by slurry nebulization and those obtained by acid digestion.

2. Experimental

2.1. Instrumentation

A laser ablation system (UP-213, ESI, Portland, OR, USA) was used for LAL sampling. A microwave acid digestion system (ETHOS One, Milestone, Sorisole, Italy) was used for decomposition of samples collected on a polycarbonate filter. ICPMS was conducted with an Agilent 7500ce instrument (Agilent Technologies, Tokyo, Japan) at settings optimized to provide the highest sensitivity for ^{7}Li, ^{89}Y, and ^{205}Tl and to keep the ^{140}Ce^{16}O/^{140}Ce ratio below 3% (Table 1). A scanning electron microscope (S-4300, Hitachi High Technologies, Tokyo, Japan) was used to observe the LAL-sampled particles. The particles were collected on a 0.4 μm polycarbonate filter, the surface of which was coated with a Pt/Pd alloy with an ion-beam sputter coater (E-1045, Hitachi High Technologies, Tokyo, Japan) prior to measurements.

2.2. LAL sampling

NIST 610 (National Institute of Standards and Technology, Gaithersburg, MD, USA) was used as a reference sample. NIST 610 contains 61 trace elements, and its matrix composition is 72% SiO_2, 12% CaO, 14% Na_2O, and 2% Al_2O_3. An open-top chamber made of PFA (tetrafluoroethylene-perfluoroalkyl vinyl ether copolymer) was used for LAL sampling. The outer diameter, inner diameter, and height of the chamber were 27, 18, and 10 mm, respectively. The NIST 610 sample was placed in the chamber, and then 1130 μL of ultrapure water (>18.2 MΩ cm, Milli-Q, Merck Millipore, Molsheim, France) was added; as a result, the surface of the sample was 3 mm below the surface of the water. The sample surface was irradiated with the laser through the water (Fig. 1). In the case of single-site mode, laser irradiation was performed for 10 min and the laser frequency was 20 Hz. The number of laser pulses was 12 000 shots for a single position. In the case of line-scanning mode, laser lines were five with 5 mm length at 200 μm intervals. The line width was 100 μm, laser frequency was 20 Hz, and scanning speed was 10 μm s^{-1}. That is, the number of laser pulses was 200 shots a single spot of 100 μm. The LAL-sampled particles suspended in the water were divided into two size classes by filtration: particles larger than 0.4 μm were collected on the polycarbonate filter, and particles smaller than 0.4 μm passed into the filtrate. The amounts of ablated particles larger than 0.4 μm and smaller than 0.4 μm were 0.057 mg and 0.15 mg, respectively.

Table 1 Operating conditions used for laser ablation in liquid inductively coupled plasma mass spectrometry (ICPMS)

Laser model	UP213
Laser type	Nd:YAG
Wavelength	213 nm
Pulse width	4 ns
Ablation mode	Single-site or line-scanning
Repetition rate	20 Hz
Diameter of the crater	100 μm
Laser fluence	6 J cm^{-2}
Scanning speed	10 μm s^{-1}
Sampling medium	Ultrapure water (1130 μL)
ICPMS model	**Agilent 7500ce**
RF power	1400 W
Integration time	0.1 s
Carrier gas (Ar) flow rate	1.2 L min^{-1}
Collision gas (He) flow rate	3.0 mL min^{-1}
Isotopes measured	^{27}Al, ^{42}Ca, ^{52}Cr, ^{55}Mn, ^{60}Ni, ^{63}Cu, ^{66}Zn, ^{69}Ga, ^{75}As, ^{85}Rb, ^{88}Sr, ^{89}Y, ^{90}Zr, ^{107}Ag, ^{111}Cd, ^{121}Sb, ^{122}Sn, ^{137}Ba, ^{157}Gd, ^{173}Yb, ^{178}Hf, ^{184}W, ^{185}Re, ^{205}Tl, ^{206}Pb, ^{209}Bi, ^{232}Th, ^{238}U

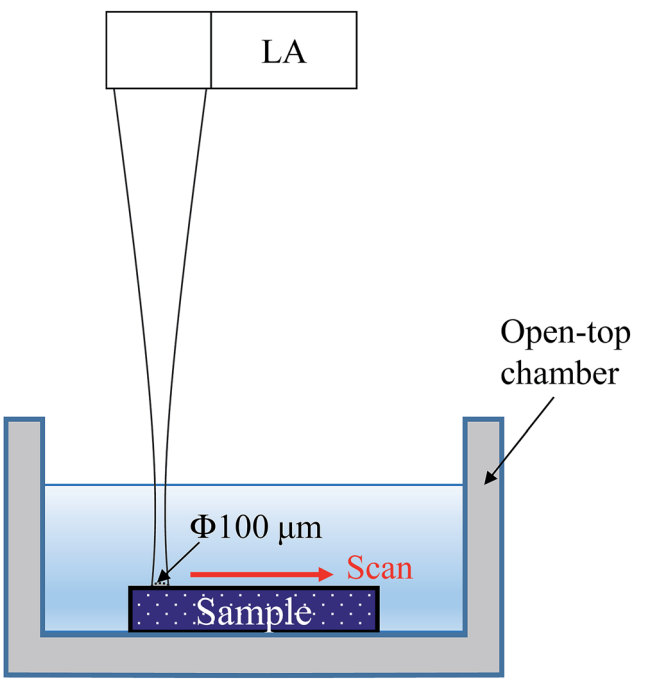

Fig. 1 Schematic diagram of laser ablation in liquid set-up. Red line indicates the scanning direction of the laser beam.

2.3. Acid digestion

NIST 610 was crushed and ground to a powder in an agate mortar. Two milligrams of the powder was weighed into a PFA vial and decomposed with a mixture of 0.3 mL of 25 M HF and 0.6 mL of 11 M HNO_3 at 180 °C on a hotplate. Heating was continued until the HF had evaporated completely, and then the digested solution was diluted to 100 mL with 0.1 M HNO_3. LAL-sampled particles were decomposed by means of the same procedure, except that a microwave digestion system was used for particles larger than 0.4 μm (that is, the particles that were collected on the polycarbonate filter). In the case of LAL-sampled particles, the final volume was adjusted to 10 mL with 0.1 M HNO_3 for particles larger than 0.4 μm and smaller than 0.4 μm. When microwave digestion was performed, a mixture of 3.0 mL of 25 M HF and 6.0 mL of 11 M HNO_3 was used.

2.4. Reagents

HF (25 M, Daikin Industries, Osaka, Japan) and HNO_3 (Ultrapure, 11 M, Kanto Chemical, Tokyo, Japan) were used in this study. Calibration standard solutions were prepared from the following SPEX multielement standards for ICPMS: XSTC-1, XSTC-7, XSTC-8, and XSTC-13 (SPEX CertiPrep, Metuchen, NJ, USA). The multielement standards were diluted with 0.1 M HNO_3. Calibration curves were prepared by measuring standard solutions at concentrations of 0, 10, 100, 500, 5000, and 10 000 pg mL^{-1}.

3. Results and discussion

3.1. Optimization of the LAL sampling procedure

The laser focus and the distance from the water surface to the sample surface were optimized carefully for LAL sampling. The focus of the CCD camera became longer with increasing distance from the water surface to the sample surface. The actual focus position of the laser beam was above the focus position of the CCD camera. The defocus adjustment, Z, can be estimated from eqn (1):

$$Z = h - a \quad (1)$$

where h is the distance between the water surface and the sample surface, and a is the apparent depth. a can be estimated from eqn (2):

$$a = \frac{h}{n} \quad (2)$$

where n is the refractive index of water (n = 1.333). The following equation (eqn (3)) could be derived from eqn (1) and (2):

$$Z = h\left(1 - \frac{1}{n}\right) \quad (3)$$

When h is 3 mm, the defocus adjustment is calculated to be 0.75 mm, indicating that the objective lens has to be moved down 0.75 mm. The optimized value of the defocus was experimentally confirmed. The images of the ablation track after LAL sampling in line-scanning mode are shown in Fig. 2. The focus was adjusted while the surface was monitored with a CCD camera. Under the in-focus condition, the width of the ablation track was 60 μm (Fig. 2a), which was narrower than the nominal value (controlled by the software at 100 μm). Under −0.50 mm defocus and −1.00 mm defocus conditions, the ablation tracks (200 and 120 μm, respectively; Fig. 2b and d) were wider than the nominal value. In contrast, under the −0.75 mm defocus condition, the width of the ablation track was equal to the nominal value (Fig. 2c).

3.2. Line-scanning mode and single-site mode

In both the line-scanning mode and the single-site mode, all of the LAL-sampled particles were decomposed, and the elemental intensities of Ca, As, Sr, Zr, Cd, Sb, Sn, Pb, Th, and U were measured by ICPMS. Enrichment factors (EFs) were calculated from eqn (4):

$$\mathrm{EF} = \left[\frac{(M_{cps}/Ca_{cps})_{LAL\text{-}sample}}{(M_{cps}/Ca_{cps})_{reference}} - 1\right] \times 100 \quad (4)$$

where $(M_{cps}/Ca_{cps})_{LAL\text{-}sample}$ is the ratio of the signal intensity of element M to that of ^{42}Ca for the sample solution obtained by LAL sampling, and $(M_{cps}/Ca_{cps})_{reference}$ is the same ratio for the sample solution obtained by decomposition of the NIST 610 powder. The EFs of these elements are shown in Fig. 3.

When the measurement was conducted in line-scanning mode, the EFs of all the elements were 0% ± 5%. In contrast, in single-site mode, the EFs of As, Cd, Sb, Sn, and Pb were −25%, −30%, −13%, −12%, and −14%, respectively; whereas the EFs of Sr, Zr, Th, and U were 0% ± 5%. In addition the aspect ratio of the crater was 0.5 when laser ablation was performed in line-scanning mode, and the aspect ratio of the crater was 4.8 when laser ablation was performed in single-site mode. More heating effect (preferential evaporation of volatile elements) occurs under higher aspect ratios.[9] Elemental fractionation was also observed in the heat effective zone under LAL.[23] Cavitation bubbles were generated at microseconds to sub-milliseconds after laser irradiation,[17] and then, nanoparticles were formed

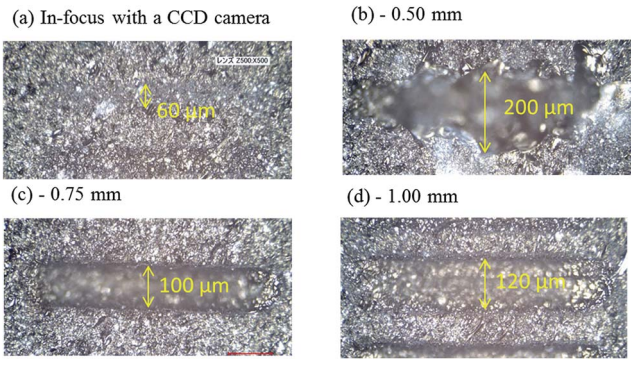

Fig. 2 CCD images of tracks of line scans: (a) in-focus with a CCD camera, (b) −0.50 mm defocus, (c) −0.75 mm defocus, and (d) −1.00 mm defocus.

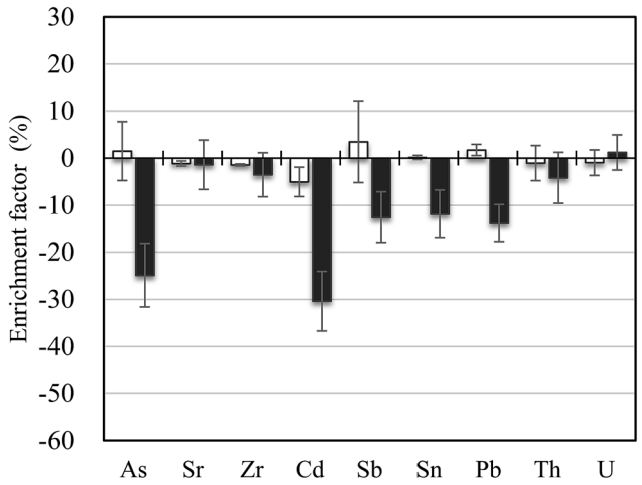

Fig. 3 Enrichment factors (%) for laser ablation in liquid sampling: (□) line-scanning mode and (■) single-site mode. Error bars indicate standard deviations ($n = 3$).

inside the cavitation bubbles.[29] In the case of single-site mode, laser irradiation heated a single spot on the sample surface, and larger cavitation bubbles were generated. Both larger aspect ratio and larger cavitation bubbles in single-site mode caused the loss of volatile elements into the gas phase *via* cavitation bubbles. This phenomenon was much clearer in single-site mode than in line-scanning mode because in the former mode, large sized cavitation bubbles were generated at a single position. Our results indicate that for quantitative analysis of elements in solid samples, LAL sampling in line-scanning mode provides more-accurate results without elemental loss. To obtain reliable data, all of the ablated particles must be collected in the liquid medium.

3.3. Dependence of elemental fractionation on the size of particles generated by LAL in line-scanning mode

LAL-sampled particles obtained in line-scanning mode were divided into two size classes by filtration: particles larger than 0.4 μm (collected on the polycarbonate filter) and particles smaller than 0.4 μm (collected in the filtrate). The scanning electron microscopy images of the two sizes of particles are shown in Fig. 4. Spherical, agglomerated, and edge-shaped particles were observed in the image of the particles on the polycarbonate filter (Fig. 4a), whereas spherical particles were the main type of particles in the filtrate (Fig. 4b). Ablated particles are generated in the heat effective zone resulting from the interaction between the sample surface and the laser beam. Larger particles are generated when hydromechanical sputtering dominates and smaller particles are generated by hydrodynamic sputtering when the heat effective zone is thin and the laser fluence is high enough for laser ablation.[30]

The elemental intensities of Ca, As, Sr, Zr, Cd, Sb, Sn, Pb, Th, and U were measured by ICPMS, and the EFs of these elements are shown in Fig. 5. In the case of the particles smaller than 0.4 μm, the EFs of As and Sb were 14% and 9%, respectively; these volatile elements were enriched by the melting–congelation process in the heat effective zone. In contrast, in the case of particles larger than 0.4 μm, the EFs of As, Cd, Sb, Sn, and Pb were −42%, −20%, −30%, −9%, and −14%, respectively. That is, the volatile elements were enriched in the LAL-sampled smaller particles, and depletion of the volatile elements was observed in the larger particles. These results imply that the degree of elemental fractionation during LAL sampling was related to the size of the ablated particles. Note that the EFs of As, Cd, Sb, Sn, and Pb were negative for particles larger than 0.4 μm, which means that these elements were depleted in these particles.

Analytical data for both sizes of LAL-sampled particles, along with the acid digestion data for the NIST 610 powder, are summarized in Table 2. The intensity values for the elements were normalized by the intensity of Ca, and the recovery percentage for each element was calculated by dividing the elemental intensity for the LAL-sampled particles by the corresponding elemental intensity for NIST 610. The recovery of all elements was 100% ± 10%. The enrichment of As, Cd, Sb, Sn, and Pb in the particles smaller than 0.4 μm and depletion of As, Cd, Sb, Sn, and Pb in the particles larger than 0.4 μm were almost balanced, within the margin of error.

Our results indicate that ICPMS analysis of LAL-sampled particles is suitable for separate study of elemental

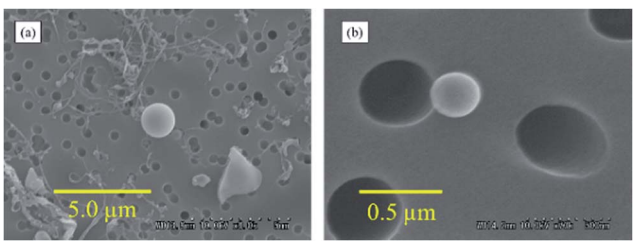

Fig. 4 Scanning electron microscopy images of the particles obtained by laser ablation in liquid sampling: (a) particles on the polycarbonate filter and (b) particles in the filtrate.

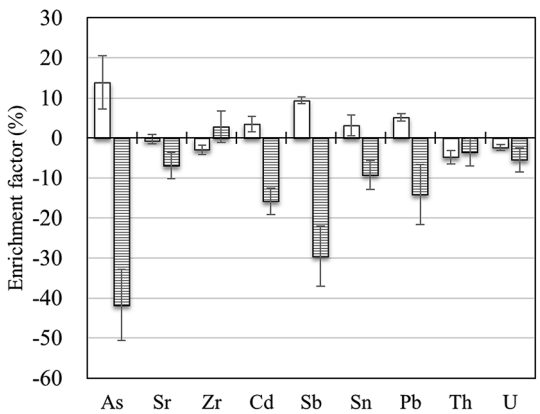

Fig. 5 Enrichment factors (%) for laser ablation in liquid sampling: (□) particles ≤0.4 μm and (▤) particles >0.4 μm. Error bars indicate standard deviations ($n = 3$).

Table 2 Intensity data obtained for LAL-sampled particles and NIST 610 powder

	LAL-sampled particles ≤ 0.4 μm			
Elements	Intensity (cps)	Intensity ratio M/Ca	Enrichment factor (%)	Enrichment (cps)
Ca	19 817	1.0	—	—
As	2732	0.14	13.9 ± 6.6	378 ± 180
Cd	2294	0.12	3.5 ± 2.4	80 ± 53
Sb	8364	0.42	9.4 ± 0.9	788 ± 75
Sn	1785	0.090	3.1 ± 2.6	55 ± 45
Pb	5335	0.27	5.1 ± 0.9	271 ± 49

	LAL-sampled particles > 0.4 μm			
Elements	Intensity (cps)	Intensity ratio M/Ca	Enrichment factor (%)	Depletion (cps)
Ca	7541	1.0	—	—
As	509	0.067	−41.8 ± 8.9	−212 ± 45
Cd	723	0.096	−20.4 ± 3.7	−147 ± 26
Sb	2060	0.27	−29.5 ± 7.6	−608 ± 155
Sn	598	0.079	−9.3 ± 3.6	−55 ± 21
Pb	1673	0.22	−14.1 ± 7.4	−236 ± 124

	Addition of data for LAL-sampled particles ≤0.4 μm and >0.4 μm		Acid digestion data for NIST 610 powder		
Elements	Intensity (cps)	Intensity ratio M/Ca	Intensity (cps)	Intensity ratio M/Ca	Recovery (%)
Ca	27 358	1.0	27 843	1.0	100
As	3241	0.12	3514	0.13	94
Cd	3017	0.11	3038	0.11	101
Sb	10 424	0.38	10 734	0.39	99
Sn	2383	0.087	2428	0.087	100
Pb	7008	0.26	7253	0.26	98

fractionation effects during LAL sampling and in the ICP. Many studies of elemental fractionation effects in LA-ICPMS have been reported,[31] but the number of papers, which described the effects that occurred during LAL sampling, during transport, and in the ICP separately, was small.[10,32]

3.4. Quantification of NIST 610 using LAL-sampling ICPMS with slurry nebulization or acid-digested-solution nebulization

The LAL-sampled particles obtained in line-scanning mode were decomposed by acid digestion, and Ag, As, Rb, Sb, Ga, Tl, Bi, Pb, Cd, Re, Sn, Cu, W, Mn, Ni, Ba, Zn, Al, Cr, Gd, Yb, Y, Sr, Zr, Hf, U, and Th were measured by ICPMS. In addition, a sample that was not subjected to acid digestion was also measured by ICPMS (by means of slurry nebulization) to investigate the effect of the particles introduced into the ICP. From the concentration of Ca, the total mass of ablated particles was estimated and all the elements other than Ca were determined. The recovery percentage for each element was calculated by dividing the concentration of the elements by the certified value of NIST 610. The analytical results and the elemental recoveries, along with the certified values, are summarized in Table 3, in which the elements are arranged in order by the melting points of their oxides. In the case of quantification by means of LAL sampling with acid digestion, the measured data were in good agreement with the certified values, and the analytical precision was <9%. These results indicate that this method is appropriate for elemental quantification in analyses involving LAL sampling.

In the case of slurry nebulization, analytical precision for the volatile elements (such as Ag, As, Rb, Ga, Tl, Cd, and Sn) was >10%. This spike noise was caused by vaporization of the volatile elements from the larger particles. The analytical precision for the other elements was <10%, except in the cases of U and Th. The reason that the analytical precision for these two refractory elements was slightly worse may have been the higher melting points of their oxides. The recoveries of Ag, As, Sb, Ga, Pb, Cd, Re, W, and Zn were >120%. These elements are vaporized more easily than Ca (the reference) because their oxides melt at much lower temperatures than does Ca oxide (2570 °C). The recovery of elements whose oxides have melting points of >1500 °C was 100% ± 20%. Elemental fractionation of these elements was small. Note that the recoveries of Cd and Zn greatly exceeded 100% in the case of slurry nebulization. The enhanced recovery of these two elements cannot be explained in terms of the melting points of their oxides, but perhaps it was due to the fact that Cd and Zn have lower boiling points (767 and 907 °C, respectively) than Ca (1484 °C). These elements were probably ionized more readily than Ca in the ICP.

Table 3 Comparison of LAL analytical data of NIST 610 glass standard obtained by slurry nebulization and acid digestion

			Slurry nebulization			Acid digestion		
Element	Certified ($\mu g\ g^{-1}$)	m.p. of oxide (°C)	Concentration ($\mu g\ g^{-1}$)	(%RSD)	Recovery (%)	Concentration ($\mu g\ g^{-1}$)	(%RSD)	Recovery (%)
Ag	254	200	390 ± 73	(18)	153 ± 19	267 ± 21	(7.8)	105 ± 8.1
As	350	274	460 ± 56	(12)	131 ± 12	346 ± 20	(5.7)	98 ± 5.9
Rb	425	412	474 ± 54	(11)	111 ± 11	439 ± 25	(5.6)	103 ± 5.7
Sb	426	570	557 ± 50	(8.9)	130 ± 9.0	416 ± 21	(5.0)	97 ± 5.2
Ga	431	660	610 ± 82	(13)	141 ± 13	462 ± 12	(2.5)	107 ± 2.7
Tl	61	717	73 ± 9.0	(12)	118 ± 12	65 ± 4.0	(6.1)	106 ± 7.3
Bi	369	817	440 ± 28	(6.3)	119 ± 6.4	396 ± 10	(2.5)	107 ± 2.5
Pb	426	897	530 ± 15	(2.8)	124 ± 2.8	434 ± 12	(2.7)	102 ± 2.9
Cd	296	900	494 ± 59	(11)	166 ± 12	298 ± 21	(7.0)	100 ± 7.3
Re	49	900	68 ± 3.6	(5.2)	138 ± 5.3	54 ± 1.7	(3.1)	108 ± 3.1
Sn	443	1080	516 ± 87	(16)	116 ± 17	471 ± 17	(3.6)	106 ± 3.8
Cu	444	1235	486 ± 14	(2.8)	109 ± 2.9	426 ± 19	(4.4)	96 ± 4.5
W	446	1500	550 ± 10	(1.8)	123 ± 1.8	458 ± 12	(2.6)	102 ± 2.6
Mn	485	1839	502 ± 4.7	(0.9)	103 ± 0.9	462 ± 8.8	(1.9)	95 ± 1.9
Ni	458	1955	476 ± 21	(4.4)	103 ± 4.4	446 ± 12	(2.6)	97 ± 2.7
Ba	458	1972	521 ± 46	(8.8)	113 ± 8.8	481 ± 13	(2.7)	105 ± 2.7
Zn	433	1974	731 ± 47	(6.4)	168 ± 6.4	470 ± 39	(8.2)	108 ± 8.3
Al	11 000	2053	10 532 ± 759	(7.2)	95 ± 7.2	11 050 ± 281	(2.5)	100 ± 2.5
Cr	411	2329	449 ± 7.5	(1.6)	109 ± 1.7	435 ± 7.1	(1.6)	105 ± 1.6
Gd	461	2339	472 ± 44	(9.3)	102 ± 9.3	488 ± 14	(2.8)	105 ± 3.0
Yb	473	2355	464 ± 20	(4.3)	98 ± 4.3	478 ± 14	(2.9)	101 ± 2.9
Y	479	2438	447 ± 34	(7.6)	93 ± 7.6	479 ± 17	(3.5)	99 ± 3.6
Sr	515	2531	541 ± 21	(3.8)	104 ± 3.9	542 ± 11	(2.0)	105 ± 2.2
Zr	473	2709	444 ± 38	(8.5)	93 ± 8.6	482 ± 18	(3.7)	101 ± 3.7
Hf	437	2774	413 ± 15	(3.6)	94 ± 3.6	439 ± 14	(3.1)	100 ± 3.3
U	461	2827	523 ± 54	(10)	113 ± 10	469 ± 15	(3.1)	101 ± 3.3
Th	457	3390	473 ± 51	(10)	103 ± 11	442 ± 14	(3.1)	96 ± 3.2

3.5. Comparison of elemental fractionation in the ICP with that during LAL sampling

LAL-sampled particles were decomposed by acid and analyzed by ICPMS. The EFs obtained by means of this procedure reflect elemental fractionation during LAL sampling. In contrast, slurry nebulization was carried out after the LAL-sampled particles were already present in the sample, and therefore the EFs obtained under these conditions reflect the elemental fractionation both during LAL sampling and in the ICP. The EFs obtained for the two sizes of LAL-sampled particles and by means of the two different analytical methods are compared in Table 4.

For volatile elements such as As, Sb, Pb, Cd, and Sn, the EFs for particles larger than 0.4 μm were negative: −41.8%, −29.5%, −14.1%, −20.4%, and −9.3%, respectively. In contrast, the EFs obtained for the samples subjected to slurry nebulization were

Table 4 Comparison of enrichment factors obtained for different sizes of LAL-sampled particles and different analytical methods

		LAL-sampled particles separated by size		Different analytical methods	
Element	Group[a]	Particles ≤ 0.4 μm (%)	Particles > 0.4 μm (%)	Slurry nebulization (%)	Acid digestion (%)
As	1	13.9 ± 6.6	−41.8 ± 8.9	39.3 ± 17.1	−6.6 ± 3.8
Sb	1	9.4 ± 0.9	−29.5 ± 7.6	26.6 ± 19.7	−8.9 ± 1.8
Pb	1	5.1 ± 0.9	−14.1 ± 7.4	20.2 ± 14.4	−4.3 ± 2.1
Cd	1	3.5 ± 2.4	−20.4 ± 3.7	58.3 ± 11.9	−2.5 ± 5.8
Sn	1	3.1 ± 2.6	−9.3 ± 3.6	14.0 ± 13.6	−6.8 ± 4.4
Sr	2	−0.3 ± 1.1	−6.9 ± 3.2	6.6 ± 3.8	−4.5 ± 1.3
Zr	2	−3.0 ± 1.2	2.8 ± 3.9	−5.2 ± 3.9	−2.1 ± 2.0
U	2	−2.3 ± 0.7	−5.5 ± 3.0	4.1 ± 4.1	−6.3 ± 1.7
Th	2	−4.8 ± 1.7	−3.6 ± 3.4	−2.7 ± 8.0	−6.2 ± 1.7

[a] Ref. 33.

positive: 39.3%, 26.6%, 20.2%, 58.3%, and 14.0%, respectively. The data of Ca intensities in Table 2 show the mass of particles corresponding to different sampling by means of LAL. The intensity data of Ca in particles smaller than 0.4 μm (19 817) were 2.6 times larger than that in particles larger than 0.4 μm (7541). That is, the mass of particles smaller than 0.4 μm was 2.6 times greater than that of particles larger than 0.4 μm. The EFs of volatile elements obtained by means of slurry nebulization were larger than addition of 2.6 times positive EFs for the LAL-sampled particles smaller than 0.4 μm plus the negative EFs for the LAL-sampled particles larger than 0.4 μm. Therefore, it was concluded that positive EFs obtained by means of slurry nebulization was caused by changes of EFs for larger particles from negative to positive values. These results indicate that the volatile elements in larger particles were depleted during LAL sampling but enriched when the particles were introduced into the ICP. Note that the magnitude of enrichment was larger than the magnitude of depletion. Therefore, we conclude that the elemental fractionation observed in the ICP was larger than that observed during LAL sampling. The EFs for Sr, Zr, U, and Th were 0% ± 7%, which suggests that these elements can be quantified without the need for considering particle size-related elemental fractionation.

The elements in Table 4 were classified into two groups on the basis of the magnitude of the EF obtained for slurry nebulization. As, Sb, Pb, Cd, and Sn were classified into group 1 because their EFs were >14%, and Sr, Zr, U, and Th were classified into group 2 because their EFs were 0% ± 7%. The classification of the elements on the basis of their EFs showed good agreement with the previously reported classification based on the fractionation index.[33]

4. Conclusions

In this study, we investigated elemental fractionation in LAL-ICPMS by separately determining the magnitude of fractionation during LAL sampling and in the ICP. LAL-ablated particles were completely collected in water under line-scanning mode. LAL-ablated particles exhibited elemental fractionation that was related to the particle size. Volatile elements were enriched in particles smaller than 0.4 μm and depleted in particles larger than 0.4 μm. Our results indicate that both positive and negative fractionation occurred during LAL sampling. Scanning electron microscopy indicated that the smaller particles were spherical. These particles were produced by melting and congelation in the heat effective zone on the sample surface. The larger particles were spherical, agglomerated, and edge shaped. Our results indicate that the volatile elements were depleted in the larger particles and enriched in the smaller particles. When all of the LAL-sampled particles were collected and analyzed by ICPMS after acid digestion, accurate and precise data were obtained, indicating that LAL sampling is a useful technique for quantitative analysis. In the case of slurry nebulization, the EFs of the volatile elements were larger than addition of 2.6 times positive EFs for the LAL-sampled particles smaller than 0.4 μm plus the negative EFs for the LAL-sampled particles larger than 0.4 μm. The results indicate that positive fractionation occurred in the ICP and that the magnitude of this fractionation was much larger than that observed during LAL sampling.

Acknowledgements

This research was supported by the Ministry of Education, Culture, Sports, Science and Technology, Japan, through a Grant-in-Aid for Scientific Research (C) (no. 26410160) and a Grant-in-Aid for Young Scientists (B) (no. 26870595). Part of this study was supported under a joint research project conducted at the Institute of Science and Engineering of Chuo University, Tokyo, Japan.

References

1 S. Kappel, S. F. Boulyga, L. Dorta, D. Günther, B. Hattendorf, D. Koffler, G. Laaha, F. Leisch and T. Prohaska, *Anal. Bioanal. Chem.*, 2013, **405**, 2943–2955.
2 J. O'Reilly, D. Douglas, J. Braybrook, P.-W. So, E. Vergucht, J. Garrevoet, B. Vekemans, L. Vinczec and H. G. Infante, *J. Anal. At. Spectrom.*, 2014, **29**, 1378–1384.
3 H. Zhou, Z. Wanga, Y. Zhu, Q. Li, H.-J. Zou, H.-Y. Qu, Y.-R. Chen and Y.-P. Du, *Spectrochim. Acta, Part B*, 2013, **90**, 55–60.
4 K. P. Jochum, B. Stoll, K. Herwig and M. Willbold, *J. Anal. At. Spectrom.*, 2007, **22**, 112–121.
5 C. O'Connor, B. L. Sharp and P. Evans, *J. Anal. At. Spectrom.*, 2006, **21**, 556–565.
6 M. Tibi and K. G. Heumann, *J. Anal. At. Spectrom.*, 2003, **18**, 1076–1081.
7 Y. Zhu, A. Hioki and K. Chiba, *J. Anal. At. Spectrom.*, 2013, **28**, 301–306.
8 T.-M. Do, H.-F. Hsieh, W.-C. Chang, E.-E. Chang and C.-F. Wang, *Spectrochim. Acta, Part B*, 2011, **66**, 610–618.
9 A. J. G. Mank and P. R. D. Mason, *J. Anal. At. Spectrom.*, 1999, **14**, 1143–1153.
10 H. R. Kuhn, M. Guillong and D. Günther, *Anal. Bioanal. Chem.*, 2004, **378**, 1069–1074.
11 I. Kroslakova and D. Günther, *J. Anal. At. Spectrom.*, 2007, **22**, 51–62.
12 T. E. Jeffries, S. E. Jackson and H. P. Longerich, *J. Anal. At. Spectrom.*, 1998, **13**, 935–940.
13 M. Ohata, D. Tabersky, R. Glaus, J. Koch, B. Hattendorf and D. Günther, *J. Anal. At. Spectrom.*, 2014, **29**, 1345–1353.
14 J. Koch, A. von Bohlen, R. Hergenröder and K. Niemax, *J. Anal. At. Spectrom.*, 2004, **19**, 267–272.
15 G. Compagnini, A. A. Scalisi and O. Puglisi, *J. Appl. Phys.*, 2003, **94**, 7874–7877.
16 O. R. Musaev, A. E. Midgley, J. M. Wrobel and M. B. Kruger, *Chem. Phys. Lett.*, 2010, **487**, 81–83.
17 V. Amendola and M. Meneghetti, *Phys. Chem. Chem. Phys.*, 2013, **15**, 3027–3046.
18 V. Amendola and M. Meneghetti, *Adv. Funct. Mater.*, 2012, **22**, 353–360.
19 H. Wu, R. Yang, B. Song, Q. Han, J. Li, Y. Zhang, Y. Fang, R. Tenne and C. Wang, *ACS Nano*, 2011, **5**, 1276–1281.

20 V. Morandi, F. Marabelli, V. Amendola, M. Meneghetti and D. Comoretto, *J. Phys. Chem. C*, 2008, **112**, 6293–6298.
21 P. Liu, Y. Liang, X. Lin, C. X. Wang and G. Yang, *ACS Nano*, 2011, **5**, 4748–4755.
22 D. N. Douglas, J. L. Crisp, H. J. Reid and B. L. Sharp, *J. Anal. At. Spectrom.*, 2011, **26**, 1294–1301.
23 S. Okabayashi, T. D. Yokoyama, Y. Kon, S. Yamamoto, T. Yokoyama and T. Hirata, *J. Anal. At. Spectrom.*, 2011, **26**, 1393–1400.
24 J. G. Williams, A. L. Gray, P. Norman and L. Ebdon, *J. Anal. At. Spectrom.*, 1987, **2**, 469–472.
25 N. S. Mokgalaka, R. I. McCrindle and B. M. Botha, *J. Anal. At. Spectrom.*, 2004, **19**, 1375–1378.
26 N. S. Mokgalaka, T. Wondimu and R. I. McCrindle, *Bull. Chem. Soc. Ethiop.*, 2008, **22**, 313–321.
27 M. Aramendia, M. Resanob and F. Vanhaecke, *J. Anal. At. Spectrom.*, 2009, **24**, 41–50.
28 Z. Wang and P. Yang, *J. Anal. At. Spectrom.*, 2014, **29**, 2091–2103.
29 T. E. Itina, *J. Phys. Chem. C*, 2011, **115**, 5044–5048.
30 R. Hergenröder, *J. Anal. At. Spectrom.*, 2006, **21**, 505–516.
31 R. E. Russo, X. Mao, H. Liu, J. Gonzalez and S. S. Mao, *Talanta*, 2002, **57**, 425–451.
32 J. Koch, I. Feldmann, N. Jakubowski and K. Niemax, *Spectrochim. Acta, Part B*, 2002, **57**, 975–985.
33 R. Machida, T. Nakazawa and N. Furuta, *Anal. Sci.*, 2015, **31**, 345–355.